This paper appears in Control Engineering Practice (A Journal of IFAC), 2018.
https://doi.org/10.1016/j.conengprac.2018.08.017

Ultrasound Image Guidance and Robot Impedance Control for Beating-Heart Surgery

Lingbo Cheng[a, *] and Mahdi Tavakoli[a]

[a]*Department of Electrical and Computer Engineering, University of Alberta, Edmonton, AB, T6G 1K7 Canada*

Abstract

A novel control method is proposed for master-slave telerobotic beating-heart surgery to solve the challenges of rapid heart motion and oscillatory haptic feedback. In this paper, the ultrasound imaging-based control algorithms are used to make the slave robot compensate for the heart motion automatically. Issues including slow sampling rate and time delay caused by ultrasound imaging are addressed by a cubic interpolation and an extended Kalman filter (EKF), respectively. Meanwhile, to provide the human operator (surgeon) a feeling of operating on an idle heart, an impedance model is designed for the master robot. The proposed method is validated through experiments.

Keywords

Motion compensation, ultrasound image, force feedback, impedance control, medical robotics, beating- heart surgery.

1 Introduction

Current practice in cardiac surgeries involves stopping the heart and placing the patient on a cardiopulmonary bypass. Robotic-assisted beating-heart surgery is a promising alternative because by allowing the heart to beat normally, it could eliminate adverse effects of cardiopulmonary bypass (Paparella et al. 2002; Angelini et al. 2002) and enables intraoperative evaluation of the heart tissue motion (Fix et al. 1993). The most prominent challenge needs to be addressed for robotic-assisted beating-heart surgery is the rapid motions of the beating heart whose movement velocity and acceleration are approximately 210 mm/s and 3800 mm/s^2, respectively (Kettler et al. 2007).

To date, robotics-assisted beating-heart surgery methods have been developed to compensate for the heart motion by both position and force. For example, Yuen et al. developed a 3D ultrasound-guided motion compensation system for beating-heart mitral valve repair (Yuen et al. 2009; Yuen et al. 2013). Kesner et al. applied a robotic catheter system combining ultrasound guidance and force control to perform cardiac tissue ablation (Kesner & Howe 2014). In (Cagneau et al. 2007), the authors implemented an iterative-learning-control-based outer control loop with an inner loop to reject disturbances caused by physiological motions. Also, by using a viscoelastic active observer, Moreira et al. presented a force control scheme to compensate for the physiological movement (Moreira et al. 2012; Moreira et al. 2014). Much of the past work used a hand-held device for surgery instead of utilizing a teleoperation system, which has been shown to offer lots of advantages in minimally invasive surgery (Bowthorpe 2015) such as more accuracy and repeatability, the facilitation of motion scaling, and the ability to telemanipulate the surgical robot over a long distance.

A teleoperation system involves a master robot that provides position commands and a slave robot that receives those commands and executes tasks on and environment (the heart tissue). In unilateral teleoperation system, the human operator not only loses physical contact with the surgical tools but also loses the sense of touch. In contrast, in bilateral teleoperation system (haptic feedback), the human operator can feel the interaction force between the slave robot and the beating heart tissue, so that human operator can efficiently manipulate the master robot to provide appropriate position commands. Additionally, with haptic feedback, both accuracy and repeatability of the forces can be improved (Kitagawa et al. 2002), and the tissue damages and undesirable trauma can be reduced (Tavakoli et al. 2007). Therefore, in this paper, the research will focus on helping the human operator in performing accurate surgical tasks on the interior areas of a beating heart by using a bilateral teleoperation system.

To provide the human operator with the most convenient and reliable assistance, two ideal behaviours are necessary for the system. One ideal behaviour of the teleoperation system is the motion compensation for the beating heart movement. By automatically synchronizing the slave robot position with the beating heart motion, the position commands exerted by the human operator will be executed on a seemingly arrested heart. In fact, the summed position of the master robot and the heart will act as the reference value for the slave robot. This can improve the precision and accuracy of beating heart surgical procedures and decrease the fatigue and exhaustion of human operator.

Another essential behaviour of the bilateral teleoperation system is the non-oscillatory haptic feedback. To avoid the induced motion phenomenon (Kuchenbecker & Niemeyer 2006), the human operator should only feel a force that one would feel when directly working on an arrested heart; that is,

*Corresponding Author.
E-mails: lingbo1@ualberta.ca, mahdi.tavakoli@ualberta.ca; phone: 780-492-8935.

the quasi-periodic heartbeat-induced forces caused by the residual position mismatch between the slave robot and the heart motion and by the slave-mounted force sensor's internal inertia should not be transmitted to the human operator. For this purpose, the unintentional oscillatory portion of the slave-heart interaction force should be filtered out (MacLachlan et al. 2012), and only the non-oscillatory portion should be transmitted to the human operator.

Telerobotics- and position- based solutions have been proposed to compensate for the fast beating heart motion. (Riviere et al. 2006; Gangloff et al. 2006; Ginhoux et al. 2005; Nakajima et al. 2014) presented various control approaches applied to track the moving heart. Due to the utilization of a high-speed camera, the systems can only be used for extracardiac surgeries. Bebek and Cavusoglu presented a model-based intelligent active relative motion cancelling algorithm (Bebek & Çavusoglu 2007). As the algorithm employed biological signals, the application of this method is limited to the extracardiac surgeries as well. To extend the applications to the intracardiac surgeries, whose environments are full of blood, our research group proposed various filters and controllers for a telerobotic system that use ultrasound images to estimate the motion of the beating heart (Bowthorpe et al. 2014a; Bowthorpe et al. 2014b; Bowthorpe & Tavakoli 2015; Bowthorpe & Tavakoli 2016a; Bowthorpe & Tavakoli 2016b). Specifically, in open-chest, intracardiac surgeries, the ultrasound transducer can be pressed against the beating heart by the surgeon to visualize the interior heart tissue and the instruments inserted into the heart through a purse-string suture (that seals the entry hole so that blood does not leak out of the heart) on the exterior heart wall. Some of the developed telerobotic systems were implemented to successfully perform anchor deployments for mitral valve annuloplasty. However, poor quality of force feedback to the human operator during tool-tissue interaction provides an inconvenient feeling for the human operator and makes the task operation difficult.

To tackle the problems of oscillatory force feedback, some researchers proposed force control architectures to compensate for the beating heart motion. Cortesao and Dominici employed a cascade model predictive control architecture with a Kalman active observer (Dominici & Cortesão 2014), and a double active observer architecture (Cortesão & Dominici 2017) to achieve beating-heart motion compensation as well as good force tracking performance. These pure force control methods always require the slave robot to come into contact with the heart tissue, which is not realistic for the whole procedures of cardiac surgeries.

In our previous research (Cheng et al. 2018), two reference impedance models were designed for the master and slave robots, respectively. By appropriately adjusting the parameters for the impedance models, the slave robot followed the position commands of the master robot (human operator) when there was no contact between surgical tool and tissue and was able to comply with the beating heart's motion during the tool-tissue interaction. However, the tradeoff between the flexibility of the slave robot and the force applied to the heart tissue restricts the system's widespread applications. Besides, as the slave robot only compensates for the fast heart's motion during contact, it would be difficult for the human operator to control the slave robot to accurately reach the specific point on the surface of the heart tissue, especially for complicated surgeries.

To simultaneously achieve motion compensation for the slave robot and non-oscillatory haptic feedback on the master robot, an ultrasound image-based position controller for the slave robot and an impedance controller for the master robot are proposed for telerobotic beating-heart surgery (Fig. 1). The paper is organized as follows. Section 2 introduces the developed system for telerobotic beating-heart surgeries. Section 3 presents the motion compensation algorithms for the slave robot using ultrasound images. Section 4 presents the algorithm for non-oscillatory haptic feedback through the master robot. Section 5 shows the experimental results. Finally, Section 6 concludes the paper.

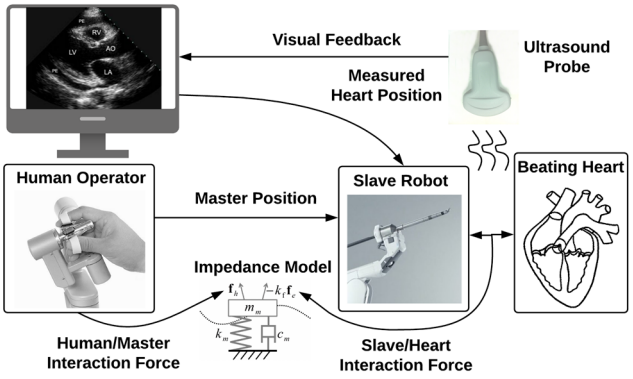

Figure 1. System concept of the proposal. The ultrasound imaging is used to compensate for the fast heart motion, and the impedance model for the master robot is proposed to achieve non-oscillatory haptic feedback.

2 Telerobotic Beating-Heart Surgical System

The developed telerobotic beating-heart surgical system to simultaneously achieve heartbeat motion compensation and haptic feedback is shown in Fig. 2. As the system needs both ultrasound images (for reading the heart tissue position) and force sensors, the position and force signals are separated by using different lines. The position signals are solid lines, and the force signals are dashed lines.

In the portion of slave block diagram, an ultrasound imaging machine is used to obtain the position of the beating heart $\mathbf{x}_e$. The summed position of the master robot $\mathbf{x}_m$ and the heart $\mathbf{x}_e$ is transmitted to the slave robot as a reference signal $\mathbf{x}_r (= \mathbf{x}_m + \mathbf{x}_e)$. And then a generalized predictive controller (GPC) is used to guarantee the position of the slave robot $\mathbf{x}_s$ follows its reference trajectory $\mathbf{x}_r$.

In the portion of the master block diagram, the interaction force between the human operator and the master robot $\mathbf{f}_h$ and the interaction force between the heart tissue and the slave robot $\mathbf{f}_e$ are transmitted directly to a reference impedance model, which will be discussed later can filter out the

high-frequency portion of $\mathbf{f}_e$ and achieve $\mathbf{f}_h$ equals the filtered $\mathbf{f}_e$. The impedance model generates a reference position $\mathbf{x}_{ref_m}$ for the master robot to follow.

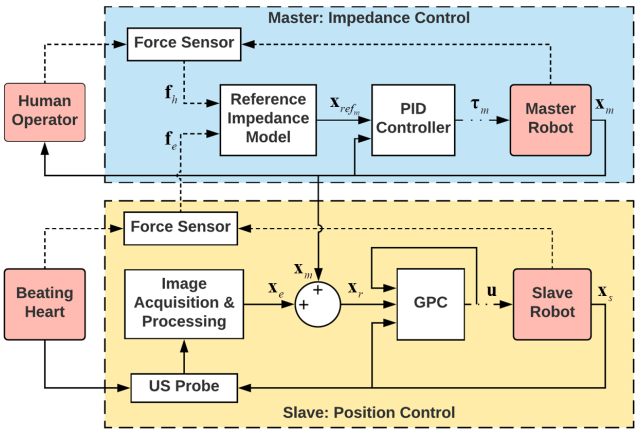

Figure 2. The telerobotic beating-heart surgical system with ultrasound image guidance and force feedback. The solid lines indicate the position transfer paths. The dashed lines indicate the force transfer paths. The dash-dotted lines are control signals.

To realize heartbeat motion compensation and non-oscillatory haptic feedback using the proposed system, there are three main problems need to be addressed:

1) *Ultrasound imaging issues: slow sampling rate and time delay.* Ultrasound machines have slow frame rates typically between 20 to 60 Hz. The force sensor, however, generally has a fast sampling rate which is more than 1000 Hz. To unify the sampling rate of the system, the position data collected at the low sampling rate of the ultrasound images should be upsampled first. In addition, the time delay caused by image acquisition and processing is not negligible and must be compensated for.

2) *Motion compensation controller.* The slave robot is designed to follow the summation of the human operator's position commands and the upsampled current heart motion. As the beating-heart motion is quasi-periodic, the future input and output signals to the slave robot can be calculated by assuming the human operator's motion is very slow. The calculated future input and output values can be taken advantage of by the controller to obtain the optimal control signal to the slave robot. Specifically, GPC is chosen to calculate the control signal over a given horizon into the future.

3) *Master robot impedance control.* To guarantee the human operator mostly perceives the slave-heart interaction forces with little feedback from the oscillatory forces through a reference impedance model, the key is to appropriately adjust the parameters of the impedance model used for the master robot.

3 Slave Robot Control: Motion Compensation Algorithm

For the sake of brevity and clarity, subsequent algorithms presented in this section will focus on the direction of the major component of heart motion. Multi-degree of freedom applications can be achieved by adjusting one axis of the slave robot frame along the direction of heart motion.

The motion compensation system is shown in Fig. 3. The designed heartbeat synchronization method requires the slave robot to follow the combined trajectory of the master robot and the beating heart. The beating-heart position can be calculated based on the position of the slave robot and the measured robot-heart distance by ultrasound machine along the surgical tool's axis. Due to the time delay caused by image acquisition and processing, the system includes two classes of data: real-time data (shown by black lines) and delayed data (shown by gray lines). The real-time positions of the master and slave robots are measured by two position sensors mounted on the robots. The measured robot-heart distance X_d^d by ultrasound images is delayed data because ultrasound image acquisition and processing are needed for that measurement.

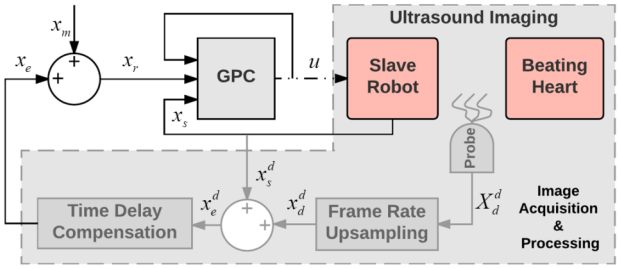

Figure 3. Motion compensation control system. Here, X_d^d indicates the measured robot-heart distance by ultrasound machine, which is slowly sampled and delayed. Also, x_d^d, x_s^d, and x_e^d are the robot-heart distance, slave robot potion, and beating heart position with a fast sampling rate, respectively. The superscript d indicates the data is delayed. The predicted beating heart position is indicated by x_e , which has both high sampling rate and no delay.

Since that the direction of x_s is set the same as the direction of the beating heart, the measured robot-heart distance X_d^d is converted to the slave robot's frame by converting it from pixels into mm. As the low sampling rate of the ultrasound image, the measured robot-heart distance X_d^d needs to be upsampled to the system control sampling rate first. And then the delayed upsampled heart position x_e^d can be obtained by delaying the position of the slave robot x_s^d and adding it to the upsampled robot-heart distance x_d^d.

To compensate for the non-negligible time delay, a predictive filter is used to predict the current heart position. In addition, a GPC is designed to obtain the control signal to the slave robot.

3.1 Image Processing

The slow sampled robot-heart distance X_d^d can be measured directly from each ultrasound image. In the following experiments, a long and thin surgical tool is mounted on the end of the slave robot to perform specific tasks. For this case, the robot-heart distance is actually the distance between the surgical tool tip and the heart tissue. To begin, each original acquired image (Fig. 4 (a)) is converted to black and white (Fig. 4 (b)) by choosing a binary threshold of 0.3. Then, a 3×3 Sobel edge detection algorithm (Sobel 1990) is used to obtain the edge points of each binary image, and a Hough transform (Duda & Hart 1972) is used to identify the longest line as the detected surgical tool. By extending this line through the surgical tool, there is an intersection of the line and the edge of the heart tissue; this intersection is the point of interest (POI) considered as the heart position. Fig. 4 (c) shows the detected edges of the surgical tool and heart tissue as well as the identified longest line and its extension. The points of surgical tool tip and POI presented in Fig. 4 (d) provide the robot-heart distance X_d^d. When the surgical tool tip makes contact with the heart tissue, the robot-heart distance is assumed to be zero.

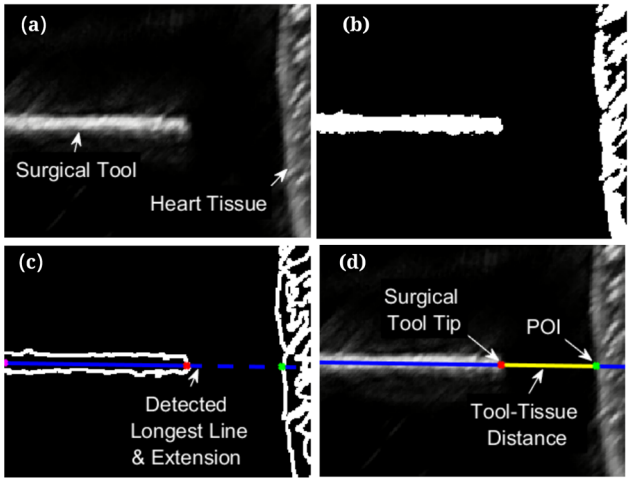

Figure 4. Image processing results. (a) The original image. (b) The converted binary image. (c) The image edges and the identified longest line and its extension using Hough transform. (d) The detected robot-heart distance between tool tip and POI in the original image.

3.2 Data Upsampling and Prediction

To begin, the measured robot-heart distance X_d^d under lower sampling rate ΔT is upsampled to a higher sampling rate Δt by using cubic spline interpolation. Consider the data points X_{d0}^d and X_{d1}^d and assume that the n points need to be added between the two data points. A third-degree polynomial, $f(i) = ai^3 + bi^2 + ci + d$, $i \in (0,1/(n+1), 2/(n+1),\cdots,1)$, can be interpolated on the interval [0,1]. The four coefficients are given by

$$\begin{aligned} a &= 2f(0) - 2f(1) + f'(0) + f'(1) \\ b &= -3f(0) + 3f(1) - 2f'(0) - f'(1) \\ c &= f'(0) \\ d &= f(0) \end{aligned} \tag{1}$$

where $f(0) = X_{d0}^d$, $f(1) = X_{d1}^d$, and $f'(0)$ and $f'(1)$ are the slopes at points X_{d0}^d and X_{d1}^d. As the calculation of $f'(1)$ requires another slowly sampled point X_{d2}^d, the total interpolation increases a processing delay of $(2n+1)\Delta t$.

To take advantage of the quasi-periodicity of the heart motion, the delayed upsampled heart position x_e^d is calculated by delaying the position of the slave robot and adding it to the upsampled robot-heart distance x_d^d. The delayed quasi-periodic heart position x_e^d is modeled as a time-varying Fourier series and predicted by an extended Kalman filter (EKF) (Jazwinski 1970) to compensate for the time delay. The state space model is expressed as

$$\begin{aligned} \mathbf{x}(t+\Delta t) &= \mathbf{A}(\Delta t)\mathbf{x}(t) + \boldsymbol{\mu}(t) \\ x_e^d(t) &= h(\mathbf{x}(t)) + v(t) \end{aligned} \tag{2}$$

In the above, $h(\mathbf{x}(t)) = c(t) + \sum_{i=1}^{m} r_i(t)\sin\theta_i(t) = c(t) + \sum_{i=1}^{m} r_i(t)\sin(i\int_0^t \omega(\tau)\mathrm{d}\tau + \phi_i(t))$ is the Fourier series of the heart motion. Here, $\mathbf{x}(t) \triangleq [c(t), r_i(t), \omega(t), \theta_i(t)]^{\mathrm{T}}$, $i \in (1, 2,\cdots, m)$, is the state vector. The first $m + 2$ state variables and $\phi_i(t)$ are assumed to evolve through random walk. Also, $\boldsymbol{\mu}(t) \sim \mathcal{N}(\mathbf{0}, \mathbf{Q})$ and $v(t) \sim \mathcal{N}(0, R)$ are the process and measurement noises, respectively.

The state transition model is

$$\mathbf{A}(\Delta t) = \begin{bmatrix} \mathbf{I}_{m+1} & & \mathbf{0} & & \\ & 1 & & & \\ & \Delta t & 1 & & \\ \mathbf{0} & 2\Delta t & 0 & 1 & \\ & \vdots & & & \ddots \\ & m\Delta t & 0 & 0 & \cdots & 1 \end{bmatrix}.$$

The Kalman filter is a recursive estimator. It uses the estimated state from the previous time step $\hat{\mathbf{x}}(t|t)$ and the 'current' heart position measurement $x_e^d(t+\Delta t)$ to compute the estimate for the 'current' state $\hat{\mathbf{x}}(t+\Delta t|t+\Delta t)$. To begin, the predicted state estimate and estimate covariance are expressed as

$$\hat{\mathbf{x}}(t+\Delta t|t) = \mathbf{A}(\Delta t)\hat{\mathbf{x}}(t|t) \tag{3}$$

$$\mathbf{P}(t+\Delta t|t) = \mathbf{A}\mathbf{P}(t|t)\mathbf{A}^{\mathrm{T}} + \mathbf{Q} \tag{4}$$

To obtain the optimal state estimate $\hat{\mathbf{x}}(t+\Delta t|t+\Delta t)$, a Kalman gain $\mathbf{K}$ is needed and given by

$$\mathbf{K} = \mathbf{P}(t+\Delta t|t)\mathbf{H}^{\mathrm{T}} / (\mathbf{H}\mathbf{P}(t+\Delta t|t)\mathbf{H}^{\mathrm{T}} + R) \tag{5}$$

Here,

$$\mathbf{H}^{\mathrm{T}}(\Delta t) = \left(\frac{\partial h}{\partial \mathbf{x}}\right)^{\mathrm{T}}\Bigg|_{\hat{\mathbf{x}}(t+\Delta t|t) = \mathbf{A}(\Delta t)\hat{\mathbf{x}}(t|t)}$$

$$= \begin{bmatrix} 1 \\ \sin\hat{\theta}_1(t+\Delta t|t) \\ \vdots \\ \sin\hat{\theta}_m(t+\Delta t|t) \\ 0 \\ \hat{r}_1(\Delta t|t)\cos\hat{\theta}_1(t+\Delta t|t) \\ \vdots \\ \hat{r}_m(\Delta t|t)\cos\hat{\theta}_m(t+\Delta t|t) \end{bmatrix}.$$

The formulas for the updated state estimate and estimate covariance are as follows

$$\hat{\mathbf{x}}(t+\Delta t|t+\Delta t) = \mathbf{K}(x_e^d(t+\Delta t) - h(\hat{\mathbf{x}}(t+\Delta t|t))) + \hat{\mathbf{x}}(t+\Delta t|t) \quad (6)$$

$$\mathbf{P}(t+\Delta t|t+\Delta t) = (\mathbf{I} - \mathbf{KH})\mathbf{P}(t+\Delta t|t) \quad (7)$$

It should be noted that the state estimate $\hat{\mathbf{x}}(t+\Delta t|t+\Delta t)$ actually has a time delay. To overcome this delay, j future points ahead are predicted, and the state vector $\hat{\mathbf{x}}(t+\Delta t|t+\Delta t)$ is propagated ahead j time steps as

$$\hat{\mathbf{x}}(t+(j+1)\Delta t) = \mathbf{A}^j(\Delta t)\hat{\mathbf{x}}(t+\Delta t|t+\Delta t) \quad (8)$$

The predicted heart position at $t+\Delta t$ can be calculated by

$$x_e(t+\Delta t) = h(\hat{\mathbf{x}}(t+(j+1)\Delta t)) \quad (9)$$

3.3 Real-time Position Tracking

With the upsampled and predicted heart motion, the slave robot can be controlled with GPC (Camacho & Bordons 2007) to follow the human operator's motions and synchronize with the beating-heart motion by taking advantage of the future input and output values. A linear or linearized dynamical model of the slave robot (a single-input single-output plant) is required to estimate the future outputs. Specifically, a multi-DOF nonlinear robot dynamics can be linearized by taking into consideration the fact that the robot moves around a setpoint in a considered task. A controlled auto-regressive integrated moving average (CARIMA) model is used to describe the slave robot dynamics

$$A(z^{-1})x_s(t) = z^{-D}B(z^{-1})u(t-\Delta t) + C(z^{-1})\frac{e(t)}{\Delta} \quad \text{with } \Delta = 1 - z^{-1} \quad (10)$$

In the above, $u(t)$ and $x_s(t)$ are the control and output sequences of the slave robot and $e(t)$ is a zero-mean white noise. In addition, D is the dead time of the system, and A, B, and C are three polynomials of orders n_a, n_b and n_c in the backward shift operator z^{-1}, respectively

$$\begin{aligned} A(z^{-1}) &= 1 + a_1z^{-1} + a_2z^{-2} + \cdots + a_{n_a}z^{-n_a} \\ B(z^{-1}) &= b_0 + b_1z^{-1} + b_2z^{-2} + \cdots + b_{n_b}z^{-n_b} \\ C(z^{-1}) &= 1 + c_1z^{-1} + c_2z^{-2} + \cdots + c_{n_c}z^{-n_c} \end{aligned} \quad (11)$$

For simplicity, $C(z^{-1})$ is chosen to be 1 for the consideration of white noise case. The cost function needs to be minimized is given by

$$J(N_1, N_2, N_u) = \sum_{k=N_1}^{N_2}\delta(k)[\hat{x}_s(t+k\Delta t|t) - \omega(t+k\Delta t)]^2 + \sum_{k=1}^{N_u}\lambda(k)[\Delta u(t+(k-1)\Delta t)]^2 \quad (12)$$

where $\hat{x}_s(t+k\Delta t|t)$ is a k step ahead prediction of the system output, $\omega(t+k\Delta t)$ is the future reference trajectory for the system, and $\Delta u(t+(k-1)\Delta t)$ is the change of the control signal. In the above, N_1 and N_2 are the minima and maximum prediction horizons, and N_u is the control horizon. Also, $\delta(k)$ and $\lambda(k)$ are two weighting factors.

The goal of this cost function is to drive the future system output $\hat{x}_s(t+k\Delta t|t)$ close to the reference value $\omega(t+k\Delta t)$ and meanwhile to minimize the change of the control signal $\Delta u(t+(k-1)\Delta t)$. Note that $\omega(t+k\Delta t)$ is approximated from the current system output $x_s(t)$towards the known reference $x_r(t+k\Delta t)$ by means of the first-order system

$$\begin{aligned} \omega(t) &= x_s(t), \\ \omega(t+k\Delta t) &= \alpha\omega(t+(k-1)\Delta t) + (1-\alpha)x_r(t+k\Delta t), \\ k &\in (1, 2, \cdots, (N_1 - N_2 + 1)) \end{aligned} \quad (13)$$

where $x_r = x_e + x_m$. Here, $x_e(t+k\Delta t)$ can be obtained from the predicted heart motion by EKF. Note that $x_m(t+k\Delta t)$ is approximately equal to $x_m(t)$ by assuming the human operator moves very slowly.

To estimate the future system output $\hat{x}_s(t+k\Delta t|t)$, the following Diophantine equation is considered:

$$1 = E_k(z^{-1})\Delta A(z^{-1}) + z^{-k}F_k(z^{-1}) \quad (14)$$

Here, E_k and F_k are two unique polynomials of orders $k-1$ and n_a, respectively.

Multiplying (11) by $\Delta E_k(z^{-1})z^k$ and considering (15), it can be obtained that

$$\begin{aligned} x_s(t+k\Delta t) = {} & E_k(z^{-1})B(z^{-1})\Delta u(t+(k-d-1)\Delta t) \\ & + F_k(z^{-1})\,x_s(t) + E_k(z^{-1})\,e(t+k\Delta t) \end{aligned} \quad (15)$$

As the degree of E_k is $k-1$, the noise terms $E_k(z^{-1})\,e(t+k\Delta t)$ are all in the future. Assuming their values are zero, the future system output $\hat{x}_s(t+k\Delta t|t)$ can be obtained as

$$\hat{x}_s(t+k\Delta t|t) = G_k(z^{-1})\Delta u(t+(k-d-1)\Delta t) + F_k(z^{-1})\,x_s(t) \quad (16)$$

where $G_k = E_kB = g_0 + g_1z^{-1} + \cdots + g_kz^{-(n_b+k-1)}$.

The prediction of $\sum_{k=N_1}^{N_2}\hat{x}_s(t+k\Delta t|t)$ can be obtained by considering

$$\mathbf{x}_s = \underbrace{\mathbf{F}(z^{-1})y(t) + \mathbf{G}'(z^{-1})\Delta u(t-\Delta t)}_{\text{past}} + \underbrace{\mathbf{Gu}}_{\text{future}} = \underbrace{\mathbf{f}}_{\text{past}} + \underbrace{\mathbf{Gu}}_{\text{future}} \quad (17)$$

where $\mathbf{x}_s = \begin{bmatrix} \hat{x}_s(t+N_1\Delta t) \\ \hat{x}_s(t+(N_1+1)\Delta t) \\ \vdots \\ \hat{x}_s(t+N_2\Delta t) \end{bmatrix}$, $\mathbf{F}(z^{-1}) = \begin{bmatrix} F_{N_1}(z^{-1}) \\ F_{N_1+1}(z^{-1}) \\ \vdots \\ F_{N_2}(z^{-1}) \end{bmatrix}$,

$$\mathbf{G}'(z^{-1})=\begin{bmatrix}(G_{N_1}(z^{-1})-g_0)z\\(G_{N_1+1}(z^{-1})-g_0-g_1z^{-1})z^2\\\vdots\\(G_{N_2}(z^{-1})-g_0-g_1z^{-1}-\cdots-g_{N_2-N_1}z^{-(N_2-N_1)})z^{N_2-N_1+1}\end{bmatrix}$$

$$\mathbf{G}=\begin{bmatrix}g_0 & 0 & \cdots & 0\\ g_1 & g_0 & \cdots & 0\\ \vdots & \vdots & \ddots & \vdots\\ g_{N_2\text{-}N_1} & g_{N_2\text{-}N_1\text{-}1} & \cdots & g_0\end{bmatrix},$$

$$\mathbf{u}=\begin{bmatrix}\Delta u(t)\\ \Delta u(t+\Delta t)\\ \vdots\\ \Delta u(t+(N_2-N_1)\Delta t)\end{bmatrix}.$$

The cost function can be written as

$$J=(\mathbf{f}+\mathbf{G}\mathbf{u}-\boldsymbol{\omega})^{\mathrm{T}}(\mathbf{f}+\mathbf{G}\mathbf{u}-\boldsymbol{\omega})+\lambda\mathbf{u}^{\mathrm{T}}\mathbf{u} \tag{18}$$

where $\boldsymbol{\omega}=\begin{bmatrix}\omega(t+N_1\Delta t)\\ \omega(t+(N_1+1)\Delta t)\\ \vdots\\ \omega(t+N_2\Delta t)\end{bmatrix}$.

By minimize (19), $\Delta u(t)$ can be calculated

$$\Delta u(t)=\mathbf{K}(\boldsymbol{\omega}-\mathbf{f}) \tag{19}$$

where $\mathbf{K}$ is the first row of matrix $(\mathbf{G}^{\mathrm{T}}\mathbf{G}+\lambda\mathbf{I})^{-1}\mathbf{G}^{\mathrm{T}}$.

4 Master Robot Control: Non-oscillatory Force Feedback

The reference impedance model for the master robot includes the human-master interaction force, the scaled slave-heart interaction force, and the desired master response trajectory (Cheng et al. 2018). The trajectories are in Cartesian coordinates. The relationships can be expressed as

$$m_m\ddot{\mathbf{x}}_{ref_m}+c_m\dot{\mathbf{x}}_{ref_m}+k_m\mathbf{x}_{ref_m}=\mathbf{f}_h-k_{\mathrm{f}}\mathbf{f}_e \tag{20}$$

where $\mathbf{x}_{ref_m}\in\mathbb{R}^{6\times1}$ is the position of the master impedance model, $\mathbf{f}_h\in\mathbb{R}^{6\times1}$ is the interaction force that the human operator applies to the master robot, $\mathbf{f}_e\in\mathbb{R}^{6\times1}$ is the interaction force that the heart applies to the slave robot. k_{f} is the force scaling factor. k_m, c_m, m_m are the virtual stiffness, damping and mass parameters of the master impedance model. The impedance parameters are set as positive so that the reference impedance model is a stable second-order differential equation.

The reference impedance model (20) should be designed to achieve $(\mathbf{f}_h-k_{\mathrm{f}}\mathbf{f}_e)\to0$ when the high frequency of the slave-heart interaction force has been filtered to avoid possible exhaustion caused by the refection of the oscillatory slave-heart interaction force to the human operator. Therefore, the stiffness parameter, k_m, of the impedance model should be chosen small, and the natural frequency of the model should be much lower than that of the beating-heart ω_{n_H} which has a range of 6.28 ~ 10.68 rad/sec; that is $\omega_{n_m}=\sqrt{k_m/m_m}$ should have a low natural frequency ($\omega_{n_m}\le0.6$ rad/sec $<<\omega_{n_H}$) (Sharifi et al. 2017). Also, the damping ratio of the impedance model ($\zeta_m=c_m/2\sqrt{m_mk_m}$) is chosen to be 0.7 so that to get a fast behavior in response to the harmonic physiological force of the human operator.

It should be noted that the proposed strategy can be used for a large range of irregular heart rates. For example, if the irregular heart motion has a rate not less than 2 rad/sec, the oscillatory portion of the tool-tissue interaction force will barely be perceived by the human operator given the adjusted ω_{n_m}. To be more specific, Fig. 5 implies that when $\omega_{n_m}<<\omega_{n_H}$, the high-frequency oscillatory force portion of $\mathbf{f}_e$ can be significantly filtered. Moreover, based on the slope (-40 dB/decade) in the Bode diagram of Fig. 5, the amplitude of the master impedance model's response with respect to the amplitude of the high-frequency portion of the slave-heart interaction force ($\mathbf{F}_e^h$) is $\left|\mathbf{X}_{ref_m}^h\right|<(\omega_{n_m}/\omega_{n_H})^2\left|k_{\mathrm{f}}\mathbf{F}_e^h/k_m\right|$. It can be seen that a small ω_{n_m} will lead to small amplitude of the master impedance model's response with respect to high-frequency inputs. In the paper, ω_{n_m} is chosen to be 0.5 rad/sec, so when ω_{n_H} is not less than 2 rad/sec, the magnitude of master impedance response with respect to the oscillatory tool-tissue interaction forces will be reduced to $\left|\mathbf{X}_{ref_m}^h\right|<0.0625\left|k_{\mathrm{f}}\mathbf{F}_e^h/k_m\right|$.

For the sake of brevity, the uncertainties of the system dynamics are not considered here. A detailed nonlinear robust adaptive impedance controller used for parametric and non-parametric uncertainties of the system is presented in (Sharifi et al. 2018). In the paper, a proportional-integral-derivative controller (PID controller) is used to guarantee the position of the master robot $\mathbf{x}_m$ to follow the reference trajectory $\mathbf{x}_{ref_m}$.

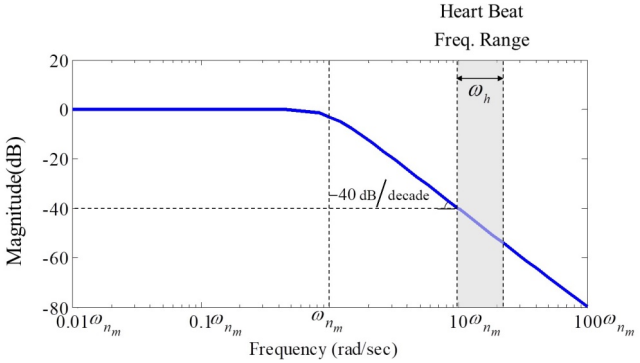

Figure 5. The Bode diagram of the reference impedance model for the master robot with natural frequency of ω_{n_m} and damping ratio of 0.7 for filtration of the high-frequency oscillatory portion of the slave-heart interaction force.

5 Experimental Evaluation

In this section, the experiments conducted in this study are described, and the validity of the proposal is confirmed. The experimental setup and the results are described in Section 5.1 and 5.2, respectively.

5.1 Experimental Setup

The experimental setup employs a Phantom Premium 1.5A robot (Geomagic Inc., Wilmington, MA, USA) as the master robot and a Quanser robot (Quanser Consulting Inc., Markham, ON, Canada) as the slave robot (Fig. 6). To measure the applied interaction forces of the surgeon and the heart tissue, the master and slave robots are respectively equipped with a 50M31 force/torque sensor (JR3 Inc., Woodland, CA, USA) and a Gamma force/torque sensor (ATI Industrial Automation, Apex, NC, USA).

A 6MHz 4dl14-5/38 linear 4D transducer connected to a SonixTouch US scanner (SonixTouch from Ultrasonix, Richmond, BC, Canada) is used as the image sensor to detect the positions of the surgical tool and the simulated heart, both of which are submerged in a water tank to represent the presence of blood inside the heart chamber. The US scanner has a low frame rate of 25 Hz. The depth of the images was 5.5 cm. The 2D US images were collected from the US scanner using a DVI2USB 3.0 frame grabber (Epiphan, Ottawa, ON, Canada). The entire image acquisition, transmission, and processing delay is 180 ms.

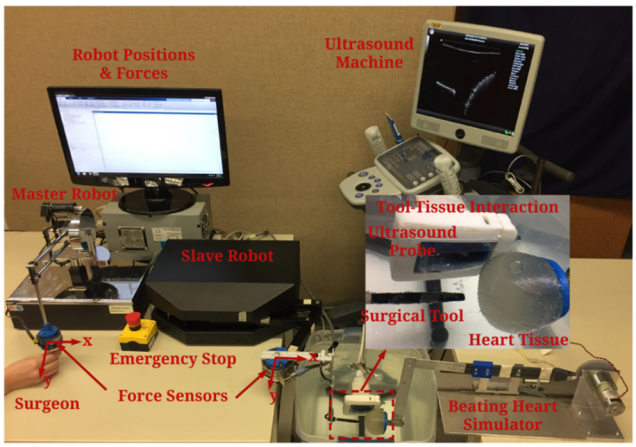

Figure 6. The experimental setup.

The heart tissue is simulated by an artificial plastisol-based tissue made of soft plastic that is visible under ultrasound. This tissue is attached to a custom-built mechanical cam which produces a peak-to-peak amplitude of 9 mm and has a fundamental frequency of 64 bpm to simulate the beating-heart motion which temporally matched to an ECG signal (Bowthorpe et al. 2014a). To verify the automated heart tissue tracking results, real-time position measurement of the beating-heart simulator was collected from a potentiometer (LP-75FP-5K from Midori America Corp., Fullerton, CA, USA). The system was controlled to perform at 1000 Hz under ultrasound guidance with the help of interpolation algorithm.

To implement the GPC system, as the heart motion is simplified to be 1DOF, only the dynamics of the slave joints that are responsible for the translation of the surgical tool along its axis (x-axis) are considered. A simplified transfer function model for the slave robot along the x-axis is identified using Matlab®. The slave robot's transfer function between the input force and the output position along x-axis can be expressed as

$$\frac{x}{F}(z^{-1}) = z^{-D}\frac{4.09 + 16.01z^{-1} + 3.977z^{-2}}{1 - 1.974z^{-1} + 0.974z^{-2}} \times 10^{-4} \tag{21}$$

Considering the system was controlled to perform at 1 KHz, the effect of discretization on the slave robot controller performance is too small to be ignored. The parameters used in the above algorithms and controllers which were obtained by trial and error during the experiments are shown in Table I.

TABLE I. EXPERIMENTAL PARAMETERS

Algorithms	Parameters Information		
	Symbol	***Definition***	***Value***
EKF	m	Harmonics number of heart motion	8
	$\mathbf{Q}$	Process noise covariance matrix	$\mathrm{diag}[0.0001_{1\times(2m+2)}]$
	R	Measurement noise covariance	0.01
	$\mathbf{P}(t_0\|t_0)$	Initial estimate covariance matrix	$\mathrm{diag}[0.001, \frac{0.1}{1}, \frac{0.1}{2}, \cdots, \frac{0.1}{m}, 0.1, 0.2_{1\times m}]$
GPC	$\lambda(k)$	Weighting factor	0.00003
	$\delta(k)$	Weighting factor	1
	D	Dead time	2
	N_1	Minimum prediction horizon	3
	N_2	Maximum prediction horizon	7
	N_u	Control horizon	5
Imp. model	ω_{n_m}	Natural frequency of impedance model	0.5 rad/sec
	k_m	Stiffness	4 N/m
	m_m	Mass	16 kg
	c_m	Damping	11.2 Ns/m
	k_f	Force scaling factor	1
PID	K_p	Proportional coefficient	1000
	K_i	Integral coefficient	200
	K_d	Derivative coefficient	1

5.2 Experimental Results

The surgical tasks in the experiments were that human operator teleoperated a slave robot to get close to, make contact with, and break contact with the simulated beating heart tissue. To verify the advantages of the proposed method compared with conventional methods, the surgical task was implemented using three methods, respectively. The first method uses a regular direct force reflection (DFR) teleoperation controller without automatic motion

compensation (AMC) (Malysz & Sirouspour 2009). This method reflects the entire slave-heart interaction force to the human operator and requires the human operator to perform motion compensation manually. The second method added AMC to the first method; thus, the force reflected to the human operator contains an oscillatory portion. The last method is the proposed strategy, which has both motion compensation and non-oscillatory force feedback.

Fig. 7 shows the actual master and slave positions and forces in the *x*-direction for the DFR teleoperation system without AMC. As seen in Fig. 7, the slave robot tracks both the position and force of the master robot during the entire operation. However, the tracking of the beating heart motion is poor as the human operator must manually compensate for the heart motion. It is very difficult for the human operator to control the oscillatory motion of the slave robot from the master site quickly enough to match the beating heart motion. Moreover, the oscillatory human-master interaction force suggests that the human operator receives unsteady haptic feedback, which makes it more challenging to synchronize the motion of the slave robot along with the beating heart motion.

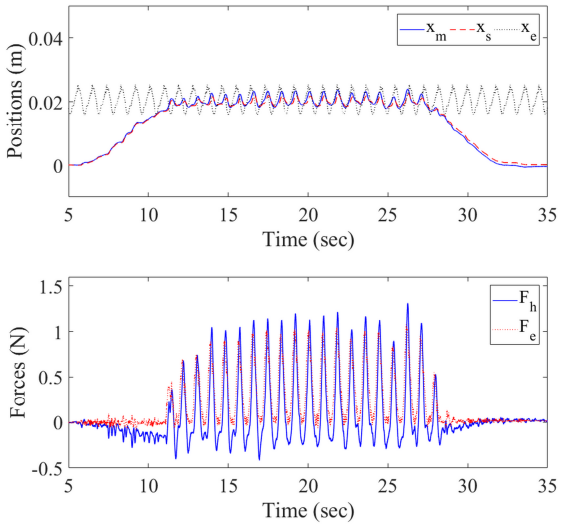

Figure 7. Position and force results for the DFR teleoperation system without AMC. In the upper position figure, the blue solid line is the position of the master robot/human operator, the red dashed line is the position of the slave robot, and the gray dotted line is the position of the heart. In the below force figure, the blue solid line is the human-master interaction force, and the red dotted line is the slave-tissue interaction force.

Fig.8 illustrates the positions and forces for the DFR teleoperation system with AMC. In this case, the slave robot is controlled to track the combined trajectory of the master robot and the heart using the proposed slave robot control scheme in Section 4. As the motion compensation is automatically achieved through the control scheme, the human operator only needs to move the slave robot towards the heart tissue. The position tracking result is much better in this case than that in the first case. Nevertheless, the haptic feedback to the human operator is still oscillatory. Meanwhile, an oscillatory motion with small amplitude remains in the master robot position due to the poor quality of haptic feedback.

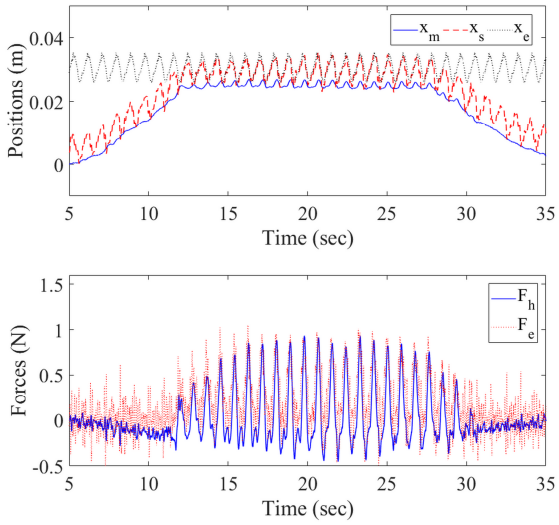

Figure 8. Position and force results for the DFR teleoperation system with AMC. In the upper position figure, the blue solid line is the position of the master robot/human operator, the red dashed line is the position of the slave robot, and the gray dotted line is the position of the heart. In the below force figure, the blue solid line is the human-master interaction force, and the red dotted line is the slave-tissue interaction force.

Using the proposed control schemes for both the master and slave robots, the results of the positions and forces are shown in Fig. 9. As seen in Fig. 9, the slave robot tracks the summed position of the human operator and the beating heart, and the position tracking result is significantly better than that in the first method. In addition, both the position and force of the master robot are much steadier as the oscillatory portions have been filtered using the proposed impedance model for the master robot. In this case, the human operator is able to operate on a beating heart without manual compensation, and at the same time, have a sense of operation on a seemingly idle heart.

In this paper, as the purpose of it is to show the feasibility of the proposed method, only three different cases are considered to present their results and discussions. In the future research, more experimental results may be presented by altering different beating rates, tissue stiffness, and impedance adjustment to show the relationships among them.

6 Conclusion

An ultrasound image-based position controller for the slave robot and an impedance controller for the master robot of are proposed for a telerobotic beating-heart surgical system to simultaneously achieve motion compensation for the slave robot and non-oscillatory haptic feedback on the master robot. The validity of the proposed method was verified through experiments, which demonstrated that the presented method

could be used in teleoperated beating heart surgeries and achieve safer and accuracy performance. Future work will involve exploring the system's use in actual beating heart procedures.

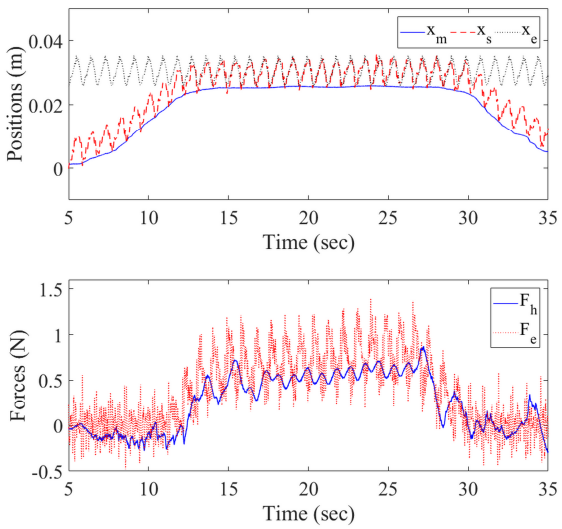

Figure 9. Position and force results for the proposed teleoperation system. In the upper position figure, the blue solid line is the position of the master robot/human operator, the red dashed line is the position of the slave robot, and the gray dotted line is the position of the heart. In the below force figure, the blue solid line is the human-master interaction force, and the red dotted line is the slave-tissue interaction force.

Acknowledgement

Research supported by the Canada Foundation for Innovation (CFI) under grant LOF 28241，the Alberta Innovation and Advanced Education Ministry under Small Equipment Grant RCP-12-021, the Natural Sciences and Engineering Research Council (NSERC) of Canada under grant RGPIN 372042, the Natural Sciences and Engineering Research Council (NSERC) of Canada under grant RGPIN 03907, and the China Scholarship Council (CSC) under grant [2015]08410152.

References

Paparella, D. et al., 2002. Cardiopulmonary bypass induced inflammation: Pathophysiology and treatment. An update. *European Journal of Cardio-thoracic Surgery*, 21(2), pp.232–244.

Angelini, G.D. et al., 2002. Early and midterm outcome after off-pump and on-pump surgery in Beating Heart Against Cardioplegic Arrest Studies (BHACAS 1 and 2): A pooled analysis of two randomised controlled trials. *Lancet*, 359(9313), pp.1194–1199.

Fix, J. et al., 1993. Do patients with less than "echo-perfect" results from mitral valve repair by intraoperative echocardiography have a different outcome? *Circulation*, 88(5 Pt 2), p.II39-48.

Kettler, D.T. et al., 2007. An active motion compensation instrument for beating heart mitral valve surgery. In *IEEE International Conference on Intelligent Robots and Systems*. pp. 1290–1295.

Yuen, S.G. et al., 2009. Robotic Motion Compensation for 3D Ultrasound-Guided Beating Heart Surgery. *The International Journal of Robotics Research*, 28(10), pp.1355–1372.

Yuen, S.G. et al., 2013. Robotic Tissue Tracking for Beating Heart Mitral Valve Surgery. *Medical Image Analysis*, 17(8), pp.1236–1242.

Kesner, S.B. & Howe, R.D., 2014. Robotic catheter cardiac ablation combining ultrasound guidance and force control. *The International Journal of Robotics Research*, 33(4), pp.631–644.

Cagneau, B. et al., 2007. Physiological Motion Compensation in Robotized Surgery using Force Feedback Control. *Proceedings 2007 IEEE International Conference on Robotics and Automation*, pp.10–14.

Moreira, P. et al., 2012. Beating Heart Motion Compensation Using Active Observers and Disturbance Estimation. In *IFAC Symposium on Robot Control International Federation of Automatic Control*. IFAC, pp. 741–746.

Moreira, P. et al., 2014. Viscoelastic model based force control for soft tissue interaction and its application in physiological motion compensation. *Computer Methods and Programs in Biomedicine*, 116(2), pp.52–67.

Bowthorpe, M., 2015. *Control for Robot-assisted Image-guided Beating-Heart Surgery*. Ph.D thesis, University of Alberta, Canada.

Kitagawa, M. et al., 2002. Analysis of Suture Manipulation Forces for Teleoperation with Force Feedback. *Fifth International Conference on Medical Image Computing and Computer Assisted Intervention*, 2488, pp.155–162.

Tavakoli, M. et al., 2007. High-fidelity bilateral teleoperation systems and the effect of multimodal haptics. *IEEE Transactions on Systems, Man, and Cybernetics, Part B: Cybernetics*, 37(6), pp.1512–1528.

Kuchenbecker, K.J. & Niemeyer, G., 2006. Induced Master Motion in Force-Reflecting Teleoperation. *Journal of Dynamic Systems, Measurement, and Control*, 128(4), pp.800–810.

MacLachlan, R.A. et al., 2012. Micron: An actively stabilized handheld tool for microsurgery. *IEEE Transactions on Robotics*, 28(1), pp.195–212.

Riviere, C. et al., 2006. Robotic Compensation of Biological Motion to Enhance Surgical Accuracy. *Proceedings - IEEE*, 94(9), pp.1705–1716.

Gangloff, J. et al., 2006. Model poredictive control for compensation of cyclic organ motions in teleoperated laparoscopic surgery. *IEEE Transactions on Control Systems Technology*, 14(2), pp.235–246.

Ginhoux, R. et al., 2005. Active filtering of physiological motion in robotized surgery using predictive control. *IEEE Transactions on Robotics*, 21(1), pp.67–79.

Nakajima, Y. et al., 2014. Heartbeat synchronization with haptic feedback for telesurgical robot. *IEEE Transactions on Industrial Electronics*, 61(7), pp.3753–3764.

Bebek, Ö. & Çavusoglu, M.C., 2007. Intelligent Control Algorithms for Robotic-Assisted Beating Heart Surgery. *IEEE Transactions on Robotics*, 23(3), pp.468–480.

Bowthorpe, M. et al., 2014a. Development of a Robotic System to Enable Beating-heart Surgery. *Journal of the Robotics Society of Japan*, 32(4), pp.23–30.

Bowthorpe, M. et al., 2014b. Smith predictor-based robot control for ultrasound-guided teleoperated beating-heart surgery. *IEEE Journal of Biomedical and Health Informatics*, 18(1), pp.157–166.

Bowthorpe, M. & Tavakoli, M., 2015. Ultrasound-Based Image Guidance and Motion Compensating Control for Robot-Assisted Beating-Heart Surgery. *Journal of Medical Robotics Research*, 1(1), 1640002.

Bowthorpe, M. & Tavakoli, M., 2016a. Generalized Predictive Control of a Surgical Robot for Beating-Heart Surgery Under Delayed and Slowly-Sampled Ultrasound Image Data. *IEEE Robotics and Automation Letters*, 1(2), pp.892–899.

Bowthorpe, M. & Tavakoli, M., 2016b. Physiological organ motion prediction and compensation based on multirate, delayed, and unregistered measurements in robot-assisted surgery and therapy. *IEEE/ASME Transactions on Mechatronics*, 21(2), pp.900–911.

Dominici, M. & Cortesão, R., 2014. Cascade Robot Force Control Architecture for Autonomous Beating Heart Motion Compensation with Model Predictive Control and Active Observer. In *IEEE RAS & EMBS International Conference on Biomedical Robotics and Biomechatronics*. pp. 745–751.

Cortesão, R. & Dominici, M., 2017. Robot Force Control on a Beating Heart. *IEEE/ASME Transactions on Mechatronics*, 22(4), pp.1736–1743.

Cheng, L. et al., 2018. Towards Robot-Assisted Anchor Deployment in Beating-Heart Mitral Valve Surgery. *International Journal of Medical Robotics and Computer Assisted Surgery*, 14(3): e1900.

Sobel, I., 1990. An isotropic 3 by 3 image gradient operator. *Machine Vision*

for three-demensional Sciences, 1(1), pp.23–34.
Duda, R.O. & Hart, P.E., 1972. Use of the Hough transform to detect lines and cures in pictures. *Communications of the Association Computing Machinery*, 15(1), pp.11–15.
Jazwinski, A.H., 1970. *Stochastic Processes and Filtering Theory*. New York: Academic Press.
Camacho, E.F. & Bordons, C., 2007. *Model predictive control*. Berlin: Springer.
Sharifi, M. et al., 2017. Tele-echography of moving organs using an Impedance-controlled telerobotic system. *Mechatronics*, 45, pp.1339–1351.
Sharifi, M. et al., 2018. Beating-heart robotic surgery using bilateral impedance control: Theory and experiments. *Biomedical Signal Processing and Control*, 45, pp.256–266.
Malysz, P. & Sirouspour, S., 2009. Nonlinear and filtered force/position mappings in bilateral teleoperation with application to enhanced stiffness discrimination. *IEEE Transactions on Robotics*, 25(5), pp.1134–1149.